Localized geomagnetic disturbance due to ionospheric response to the Hunga Tonga eruption on January 15, 2022

Gabriel Soares[1], Yosuke Yamazaki[2], and Jürgen Matzka[2]

[1] Observatório Nacional, Rio de Janeiro, Brazil.

[2] GFZ German Research Centre for Geosciences, Potsdam, Germany.

Corresponding author: Yosuke Yamazaki (yamazaki@gfz-potsdam.de)

Key Points:

- The Hunga Tonga-Hunga Ha'apai volcano in the Pacific Ocean erupted on January 15, 2022, and its effect on the geomagnetic field is examined.
- Following the eruption, localized geomagnetic pulsation-like disturbances are observed at nearby station with periods of 3-5 minutes.
- The results provide the first evidence and characterization of ionospheric effects associated with the Hunga Tonga eruption.

Abstract

The Hunga Tonga-Hunga Ha'apai volcano in the Pacific Ocean erupted on January 15, 2022. The energy released by this submarine eruption caused waves propagating through the lithosphere, ocean and atmosphere. Less than 10 minutes after the eruption, pulsation-like geomagnetic disturbances started at the geomagnetic observatory Apia, approximately 835 km from Hunga Tonga, and lasted for about 2 hours. These disturbances were most prominent in the Y (east) component, with an oscillation amplitude of ~3 nT and dominant periods of 276, 254 and 219 s. Comparable geomagnetic disturbances are absent at neighboring as well as high-latitude geomagnetic observatories, indicating that the disturbances are localized and not related to solar wind energy input. Tide gauge data show that tsunami waves arrived at Apia more than one hour after the eruption. This leaves ionospheric currents as the likely cause of the geomagnetic disturbances.

Plain Language Summary

On January 15, 2022, the Hunga Tonga-Hunga Ha'apai volcano erupted in the Pacific Ocean. Examining such an extreme event is of great interest for the geoscience community, as it can affect the Earth system in different ways. In this study, we investigate the impact of the Hunga Tonga eruption on the Earth's magnetic field. Following the eruption, geomagnetic disturbances were observed at the neighboring observatory, Apia (Western Samoa), lasting for about 2 hours with dominant period of oscillation at 3 to 5 minutes. No similar geomagnetic disturbances were detected at other neighboring observatories. The inspection of the data suggests that the disturbances observed at Apia are unlikely to be caused by enhanced geomagnetic storm activity or due to electromagnetic induction by tsunami waves. Electric currents in the ionosphere driven by atmospheric disturbances caused by the eruption are suggested as the likely cause.

1. Introduction

Geophysical events, such as earthquakes and volcanic eruptions, can provide an opportunity to test and improve our understanding of the Earth system. On January 15, 2022, the submarine volcano Hunga Tonga-Hunga Ha'apai (20.5°S, 175.4°W, Tonga) erupted in the Pacific Ocean at 04:14:45 UT. This paper examines the impact of this extreme event (hereafter denoted the Hunga Tonga eruption) on the geomagnetic field observed at selected ground stations. There are multiple reasons why the geomagnetic field might be affected by the Hunga Tonga eruption. Firstly, atmospheric disturbances caused by the eruption can propagate from the source region in the form of atmospheric waves, which reach upper layers of the atmosphere and drive electric currents in the ionosphere (e.g., Aoyama et al., 2016). Secondly, the motion of the electrically conductive ocean by tsunami waves can drive an ocean dynamo and associated geomagnetic variations, which have been reported for a number of tsunami events (see the review by Minami et al., 2017). Thirdly, the vibration of the ground by seismic waves and resulting changes in the orientation of magnetic sensors can cause spurious variations in the magnetic records.

Geomagnetic variations usually are dominated by disturbances due to solar and magnetospheric forcing. The geomagnetic Dst index, which is a measure of the magnitude of geomagnetic storms, turned negative at 17:00 UT on January 14, 2022, and reached a minimum value of -94 nT at 23:00 UT on January 14, 2022. Thus, the Hunga Tonga eruption occurred during the recovery phase of this geomagnetic storm. Geomagnetic storms and accompanying substorms can cause geomagnetic disturbances over a wide range of periods, that could potentially overlap with the geomagnetic effects of the Hunga Tonga eruption. Thus, caution needs to be exercised when interpreting the geomagnetic data so that storm-related disturbances will not be mistaken as the effect of the Hunga Tonga eruption.

2. Data

Ground-based 1 Hz magnetometer data from the following geomagnetic observatories were obtained from the INTERMAGNET network to investigate the geomagnetic response to the Hunga Tonga eruption: Apia (API, 13.8°S, 171.8°W), Pamatai (PPT, 17.6°S, 149.6°W), Charters Towers (CTA, 20.1°S, 146.3°E), Honolulu (HON, 21.3°N, 158.0°W), and Macquarie Island (MCQ, 54.5°S, 159.0°E). Figure 1a shows the location of the Hunga Tonga volcano (red triangle) and the five selected geomagnetic observatories (yellow circles). API is the closest observatory to Hunga Tonga, located 835 km north-northeast of the volcano. PPT, CTA and HON are neighbouring observatories with respective distances to the volcano of 2730 km (east of Hunga Tonga), 3990 km (west) and 4995 km (north-northeast). MCQ, 4350 km south-southwest from Hunga Tonga, is located in the auroral zone (59.4° geomagnetic latitude), where the geomagnetic field is especially susceptible to disturbances of solar and magnetospheric forcing. Figure 1a also shows the wave front of the seismic P-wave at different times indicated by white curves for 04:16:56 UT, 04:20:43 UT and 04:25:54 UT, based on the P-wave arrival times at seismic stations in Raoul, Kermadec Islands (29.3˚S, 177.9˚W), Kiritimati Island (2.0˚N, 157.5˚W) and Rapanui, Easter Island (27.1˚S, 109.3˚W), respectively; the seismic information was provided by the Incorporated Research Institutions for Seismology (IRIS).

To infer the arrival time of tsunami waves at API, 1-minute sea level data from the Apia Upolu tide gauge station (13.8°S, 171.8°W), provided by the Sea Level Station Monitoring Facility of the Intergovernmental Oceanographic Commission (IOC), are also used.

3. Results

Figures 1b-1f present the eastward (Y) component of the geomagnetic field observed at API, PPT, HON, CTA, and MCQ during the period from 12:00 UT on January 14, 2022 to 00:00 UT on January 16. In Figures 1b-1f, the top panel shows the raw data, the middle panel shows the data after band-pass filtering it in the period range of 5 to 600 s and the bottom panel shows the Morlet wavelet spectrum of the data. For the wavelet spectrum, tick marks are placed at 5, 10, 45, 150 and 600 s to indicate the period range of magnetic pulsations Pc2 (5 to 10 s), Pc3 (10 to 45 s), Pc4 (45 to 150 s) and Pc5 (150 to 600 s) (e.g., McPherron, 2005). An additional tick mark is placed at 300 s (5 minutes). The vertical dashed line in magenta indicates the beginning of the geomagnetic storm with the first negative value of the Dst index at 17:00 UT on January

14. The other vertical dashed line, black in the top and middle panels and white in the bottom panel, marks the onset of the Hunga Tonga eruption at 04:14:45 UT on January 15.

The results for API in Figure 1b reveal a geomagnetic disturbance starting shortly after the Hunga Tonga eruption (04:14:45 UT on January 15, black/white dashed line). As seen in the band-pass filtered data, this disturbance lasted for approximately 2 hours, until about 06:00 UT, and have an amplitude of up to ~3 nT. The wavelet spectrum indicates periods within the Pc5 range (150−600 s). During the quiet periods before the onset of the geomagnetic storm (17:00 UT on January14, magenta dashed line), the band-pass filtered data show only small variation of +/-0.2 nT. During the storm, the variation is larger, +/-0.5 nT, but is still much smaller than the geomagnetic disturbance in the two hours following the Hunga Tonga eruption.

The results obtained for the other observatories (PPT, HON, CTA and MCQ) are shown in Figures 1c−1f. Unlike the results for API (Figure 1b), there is no clear indication of enhanced geomagnetic disturbance in the Pc5 band following the Hunga Tonga eruption, suggesting that the geomagnetic disturbance observed at API is highly localized. An overall enhancement of geomagnetic activity following the geomagnetic storm is seen at all the stations, most profoundly at MCQ in the auroral zone. Also, a transient magnetic disturbance is visible at all the stations including API around 18:00 UT on January 15, that could be a Pi2 pulsation associated to substorm activity.

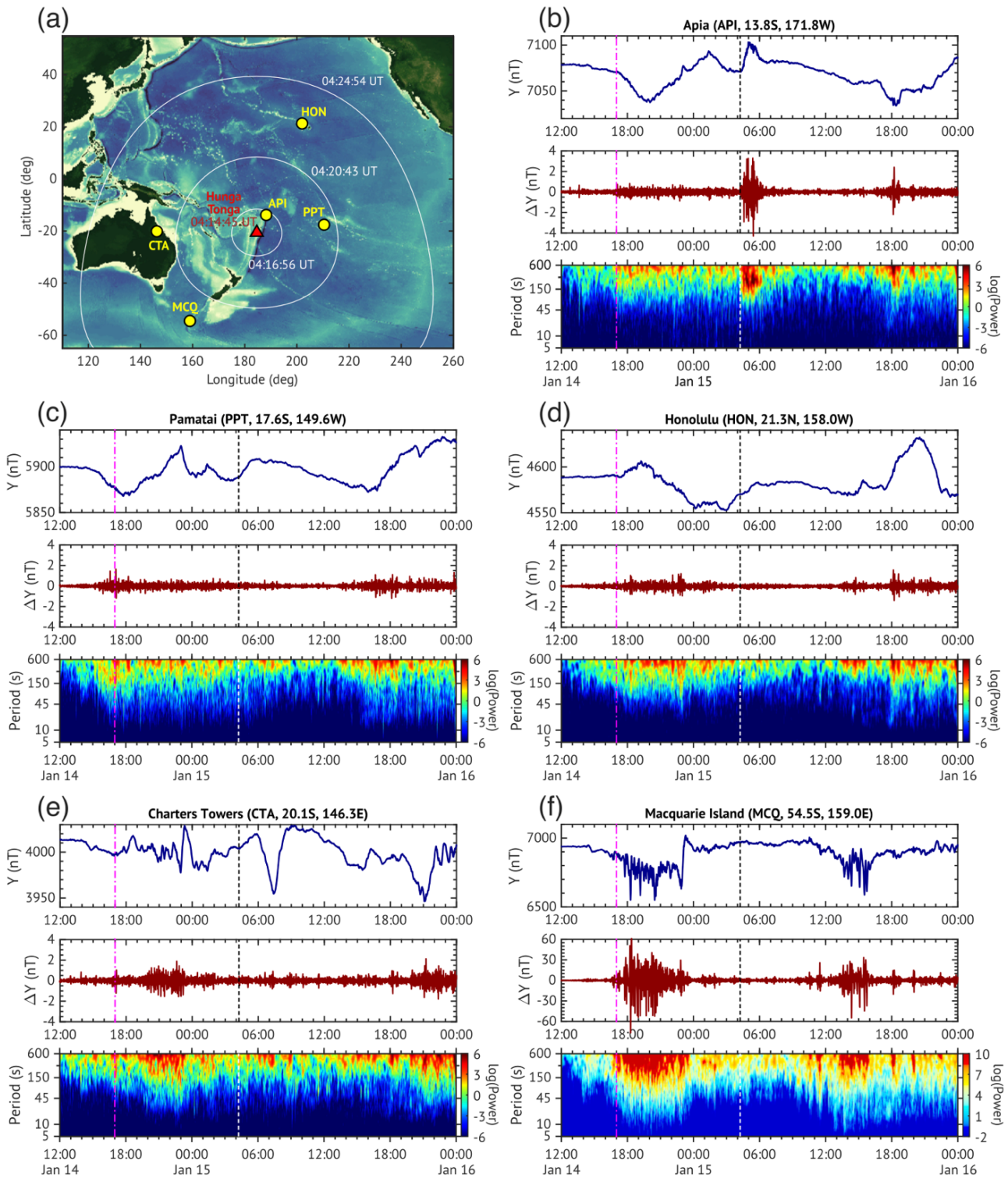

Figure 1. (a) A map with the positions of the Hunga Tonga volcano (red triangle), geomagnetic observatories (yellow circles) and the wave front of seismic P-wave (white curved lines). The land topography and ocean bathymetry are based on ETOPO1 (Amante and Eakins, 2009). (b–f) The Y component of the geomagnetic field (top), band-pass filtered data at periods 5–600 s (middle) and wavelet spectrum (bottom) for API, PPT, HON, CTA and MCQ observatories.

Results for MCQ are presented with different scales than those at the other stations. Vertical dashed lines indicate the beginning of the geomagnetic storm (magenta) and the Hunga Tonga eruption (black/white).

4. Discussion and Summary

The localized geomagnetic disturbance at API following the Hunga Tonga eruption is distinguishable from those associated with the geomagnetic storm, but its source is still unclear. As mentioned before, the disturbance could be related to magnetic fields generated by tsunami waves, atmospheric waves, or could even be an artefact caused by changes in the orientation of magnetometer sensors due to ground vibration by seismic waves.

To better describe the localized geomagnetic disturbance at API, Figure 2a shows high-pass filtered data with a cut-off period of 30 min in the X, Y, Z and F components during the period 04:00−06:30 UT on January 15, 2022. Again, the vertical dashed line indicates the time of the eruption. Ten minutes after the eruption, at 04:25 UT, pulsation-like oscillations are already visible in the Y component. The oscillation is seen to continue until around 06:00 UT. The magnetic field in the Z component shows a similar oscillation as in the Y component, but the amplitude is smaller by approximately 52% and is of opposite phase. Oscillations in the X component are less clear.

Corresponding high-pass filtered data from the tide gauge at Apia is shown in Figure 2b. The tsunami waves arrived at Apia around 05:30 UT, which is almost one hour after the start of the geomagnetic disturbance at API around 04:25 UT. Previous studies have shown that magnetic variation related to tsunami waves starts nearly at the same time as the arrival of the tsunami waves (e.g., Manoj et al., 2011; Schnepf et al., 2016). Also, tsunami-related geomagnetic variations in the Z component are expected to have a wave form similar to that of the variation of the sea level (e.g., Lin et al., 2021). In Figure 2, however, there is no similarity between the variations in the Z component and sea level even after the arrival of tsunami waves at Apia. This rules out tsunami waves as the main cause of the geomagnetic disturbances observed at API following the Hunga Tonga eruption.

As indicated in Figure 1a, seismic waves arrived at Apia around 2 minutes after the Hunga Tonga eruption. Ground motion due to the seismic waves could affect the orientation of the fluxgate sensors that measure the geomagnetic vector components and thus introduce spurious variation in X, Y and Z. The total field $F = (X^2 + Y^2 + Z^2)^{0.5}$ calculated from the vector components is far less susceptible to ground motion as it is invariant to sensor rotation. Additionally, the total field F can be measured by an overhauser magnetometer, which is also less susceptible to ground motion effects because its measurement principle does not require any specific sensor orientation. In Figure 2a, F data come from an overhauser magnetometer, and it shows pulsation-like disturbance similar to that in the Y and Z components, confirming that the geomagnetic disturbance observed at API after the Hunga Tonga eruption is not an artefact due to ground shaking. Total field F values calculated from the vector components present nearly identical variations (not shown here), leading to the same conclusion.

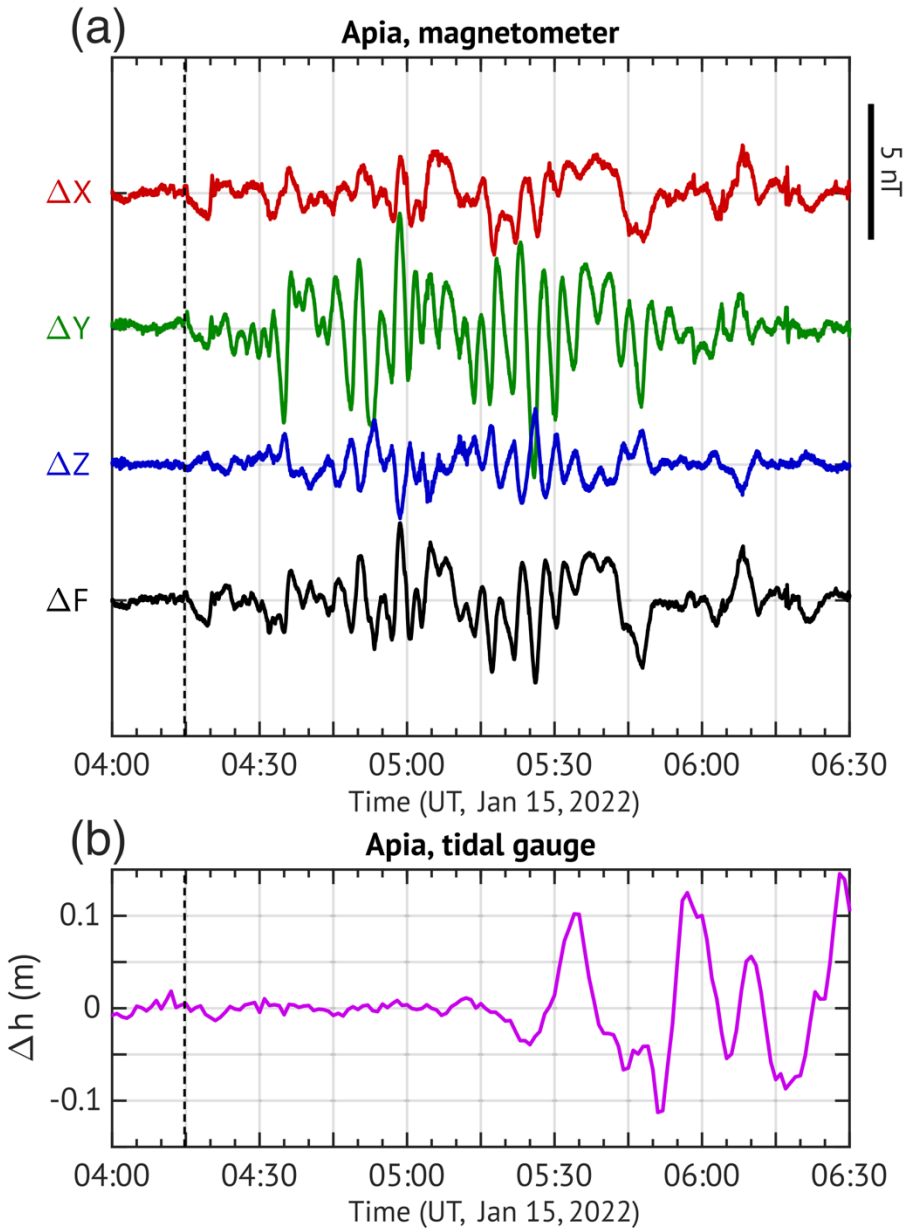

Figure 2. (a) High-pass filtered magnetometer data for API with a cutoff period of 30 minutes during 04:00−06:30 UT on January 15, 2022. (b) Same as (a) but for sea level data from the Apia tide gauge, indicating the arrival of tsunami waves around 05:30 UT. The vertical black dashed lines indicate the time of the Hunga Tonga eruption.

Atmospheric waves are another possible source of geomagnetic disturbances. Although atmospheric waves themselves do not involve electric currents, their interaction with ionospheric plasma in the dynamo region at altitudes of approximately 100 to 150 km can lead to electric currents through the mechanism known as ionospheric wind dynamo (e.g., Richmond, 1995). A condition that needs to be satisfied for the ionospheric wind dynamo to be effective is that the

dynamo region receives the sunlight so that ionospheric plasma density is sufficiently high to support electric currents. The solar zenith angle at the location of Hunga Tonga remained < 100˚ during 04:00−06:30 UT (16:18−18:48 LT), indicating that the dynamo region was on the sunlit side.

An atmospheric wave can drive dynamo currents that oscillate with the same period as the wave. Figure 3a (black line) shows the Lomb-Scargle power spectral density (PSD) estimate derived from the Y component of the geomagnetic field at API during 04:15 to 06:15 UT on January 15, 2022, when the geomagnetic disturbance following the Hunga Tonga eruption is most pronounced. The three most dominant periods are 276 s (4.60 minutes), 254 s (4.24 minutes) and 219 s (3.66 minutes). The green lines show the results obtained from the API geomagnetic Y component over two-hour segments but at different UTs and days within an interval of +/- 10 days from the eruption event, representing the background PSD level. The results suggest that oscillations at 3 to 5 minutes are not common outside the two-hour event following the eruption. Figures 3b and 3c display spectra for the Z and X components, respectively. After the eruption, the Z component shows a spectral pattern similar to the Y component, while in the X component, oscillations at 3 to 5 minutes are not evident.

Geomagnetic oscillations at periods of 3 to 5 minutes have been previously reported for other extreme geophysical events. For instance, Iyemori et al. (2005) observed a magnetic oscillation with a period of 3.6 minutes (216 s) after the December 2004 Sumatra earthquake. Aoyama et al. (2016) observed magnetic oscillations at 3 to 5 minutes, the most prominently at 4.3 minutes (258 s), following the Calbuco volcano eruption in April 2015. In both studies, the geomagnetic effects are attributed to ionospheric sources. The period of 3 to 5 minutes can be explained by acoustic resonant oscillations of the atmosphere between the ground and thermosphere (e.g., Kanamori et al., 1994; Lognonné et al., 1998). The acoustic waves excited by the eruption would propagate upward at the speed of sound (~340 m/s) and reach the dynamo region above the volcano within 10 minutes (e.g., Rolland et al., 2011). This enables the fast response of the ionosphere (and hence geomagnetic field) to the eruption, as seen in Figure 2.

Zettergren and Snively (2013, 2015) numerically demonstrated that acoustic waves generated near the surface can drive localized ionospheric currents above the source in the direction parallel to the magnetic field lines. Since the geomagnetic declination at Hunga Tonga is relatively small (ca 14˚), ionospheric currents parallel to the geomagnetic field lines would produce ground geomagnetic perturbations mainly in the Y component. The magnetic perturbations in the Z component are absent right below the field-aligned currents, but non-zero at either the eastern or western side of the currents. Since API is located about 100 km east to the magnetic meridian of Hunga Tonga, northward/upward field-aligned currents over Hunga Tonga would generate a negative perturbation in the Y component and a positive perturbation in the Z component. This can explain why the magnetic variations at API in the Y and Z components are of opposite phase (Figure 2a).

Based on the above discussion, we conclude that ionospheric currents are the likely cause of the geomagnetic disturbance at API following the Hunga Tonga eruption. This is the first time that evidence of ionospheric effects associated with the Hunga Tonga eruption is presented. The amplitude of the geomagnetic oscillations at API is up to ~3 nT, which is much greater than those previously reported for other earthquakes (e.g., ~0.5 nT in Iyemori et al., 2005) and other

volcanic eruptions (e.g., ~0.2 nT in Aoyama et al., 2016). This is the first time that such large magnetic signatures from the ionosphere are detected during an eruption event. The large amplitude is probably owing to both the strong ionospheric currents involved and the proximity of API to Hunga Tonga.

More studies are warranted, as many questions remain open. For example, the three-dimensional structure of the ionospheric current system responsible for the geomagnetic disturbances is still unclear. Also, atmospheric waves responsible for different peaks in the spectrum of the geomagnetic disturbances (Figure 3) need to be identified. Broader effects are expected in other ionospheric parameters such as total electron content (e.g., Astafyeva, 2019), which also need to be explored in future work.

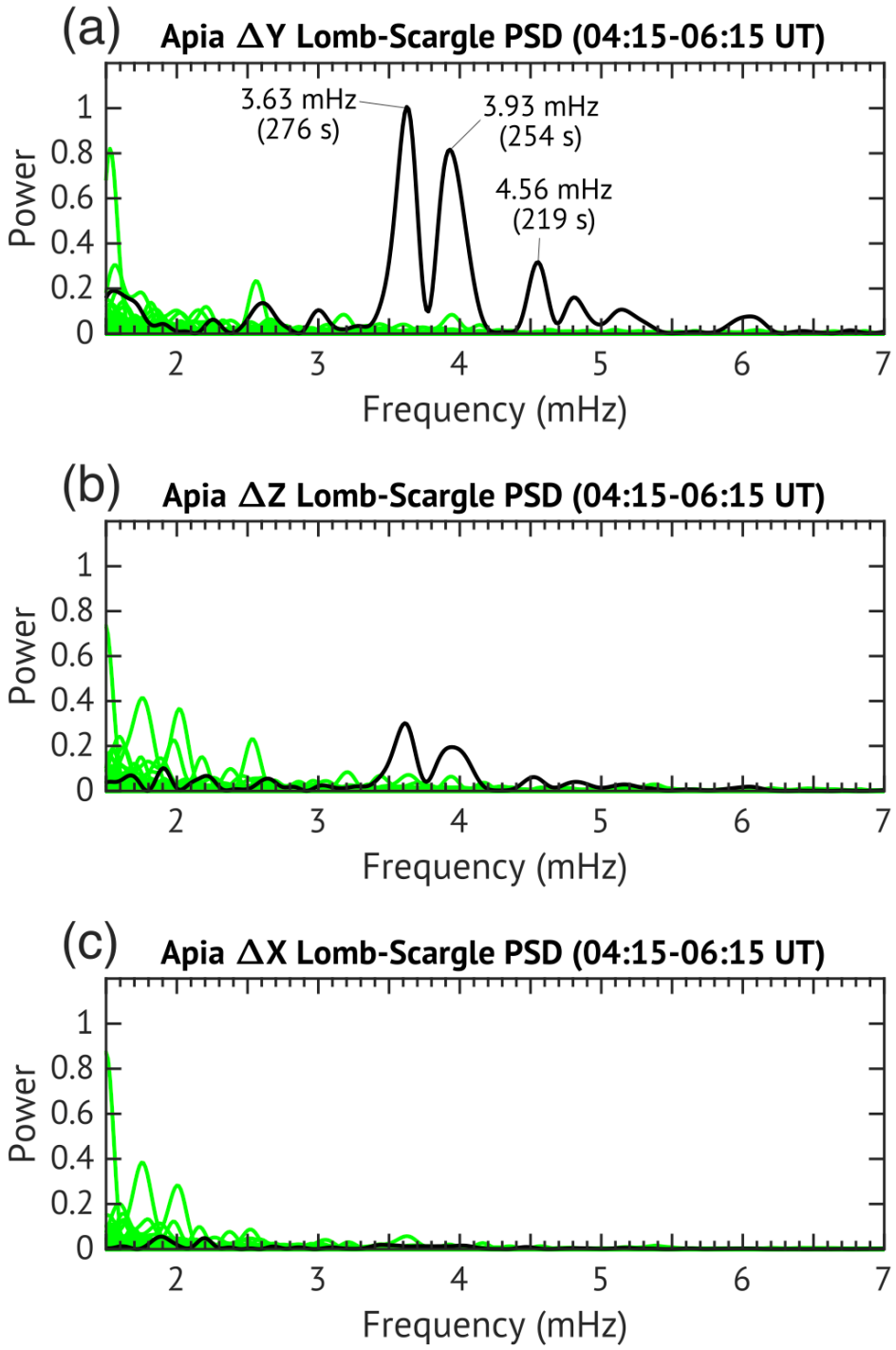

Figure 3. Lomb-Scargle power spectral density (PSD) estimates for the (a) Y, (b) Z and (c) X components of the geomagnetic field at API in arbitrary normalized units. The PSD for the two-hour interval 04:15−06:15 UT on January 15, 2022, representing the Hunga Tonga event disturbance, is shown in black. Dominant periods are 276 s (4.60 minutes), 254 s (4.24 minutes) and 219 s (3.66 minutes). All other two-hour intervals within +/−10 days from the eruption event, representing the background PSD level, are show in green.

Open Research

The geomagnetic data used in this paper are available at the INTERMAGNET website (https://www.intermagnet.org/data-donnee/download-eng.php). The sea level data for Apia Upolu on January 15, 2022 are available at the IOC website (http://www.ioc-sealevelmonitoring.org/bgraph.php?code=upol&output=tab&period=1&endtime=2022-01-16); see also data publication (Flanders Marine Institute (VLIZ); Intergovernmental Oceanographic Commission (IOC), 2021).

Acknowledgements

The results presented in this paper are based on the long-term observations made at geomagnetic observatories and tide gauges. We acknowledge the Ministry of Natural Resources & Environment – Meteorology Division (MNRE), Samoa, and GNS Science, New Zealand for operating API and ETH Zurich, Switzerland, the United States Geological Service (USGS) and GFZ Potsdam for supporting it. We thank Institut de Physique du Globe de Paris (IPGP) for operating PPT, the United States Geological Survey (USGS) for operating HON and Geoscience Australia (GA) for operating CTA and MCQ. INTERMAGNET is acknowledged for promoting high standards of geomagnetic observatory practice. We acknowledge WDC Kyoto for providing the Dst index and the Sea Level Station Monitoring Facility of the IOC for providing sea water level data. We also acknowledge the IRIS for making the seismic information available. G.S. was supported by the Coordenação de Aperfeiçoamento de Pessoal de Nível Superior – Brasil (CAPES) – Finance Code 1799579. Y.Y. was supported by the Deutsche Forschungsgemeinschaft (DFG) grant YA-574-3-1. J.M. was supported by DFG (grant MA-2578-4-1) in the framework of Priority Program 1788 'DynamicEarth'.

References

Amante, C. & Eakins B.W. (2009). ETOPO1 1 arc-minute global relief model: Procedures, data sources and analysis. NOAA Technical Memorandum NESDIS NGDC-24. National Geophysical Data Center, NOAA. https://doi.org/10.7289/V5C8276M.

Aoyama, T., Iyemori, T., Nakanishi, K., Nishioka, M., Rosales, D., Veliz, O. & Safor, E.V. (2016). Localized field-aligned currents and 4-min TEC and ground magnetic oscillations during the 2015 eruption of Chile's Calbuco volcano. Earth Planet and Space, 68. https://doi.org/10.1186/s40623-016-0523-0.

Astafyeva, E. (2019). Ionospheric detection of natural hazards. Reviews of Geophysics, 57(4), 1265-1288. https://doi.org/10.1029/2019RG000668

Flanders Marine Institute (VLIZ); Intergovernmental Oceanographic Commission (IOC) (2021): Sea level station monitoring facility. Accessed at http://www.ioc-sealevelmonitoring.org on 2021-05-22 at VLIZ. DOI: 10.14284/482

Iyemori, T., Nose, M., Han, D., Gao, Y., Hashizume, M., Choosakul, N., Shinagawa, H., Tanaka, Y., Utsugi, M., Saito, A., McCreadie, H., Odagi, Y & Yang, F. (2005). Geomagnetic pulsations caused by the Sumatra earthquake on December 26, 2004. Geophysical Research Letters, 32(20). https://doi.org/10.1029/2005GL024083

Kanamori, H., Mori, J., & Harkrider, D. G. (1994). Excitation of atmospheric oscillations by volcanic eruptions. Journal of Geophysical Research: Solid Earth, 99 (B11), 21947-21961, https://doi.org/10.1029/94JB01475

Lin, Z., Toh, H., & Minami, T. (2021). Direct comparison of the tsunami- generated magnetic field with sea level change for the 2009 Samoa and 2010 Chile tsunamis. Journal of Geophysical Research: Solid Earth, 126, e2021JB022760. https://doi.org/10.1029/2021JB022760

Lognonné, P., E. Clévédé, & Kanamori H. (1998). Computation of seismograms and atmospheric oscillations by normal-mode summation for a spherical Earth model with realistic atmosphere, Geophysical Journal International, 135, 388–406. https://doi.org/10.1046/j.1365-246X.1998.00665.x

Manoj, C., Maus, S., & Chulliat, A. (2011) Observation of magnetic fields generated by tsunamis. EOS, Transactions, American Geophysical Union, 92:13. https://doi.org/10.1029/2011EO020002

McPherron, R. L. (2005). Magnetic Pulsations: Their Sources and Relation to Solar Wind and Geomagnetic Activity. Surveys in Geophysics 26, 545–592. https://doi.org/10.1007/s10712-005-1758-7

Minami, T. (2017). Motional Induction by Tsunamis and Ocean Tides: 10 Years of Progress. Surveys in Geophysics, 38, 1097–1132. https://doi.org/10.1007/s10712-017-9417-3

Richmond, A. D. (1995). Ionospheric electrodynamics. In: Volland, H. (Ed.), Handbook of atmospheric electrodynamics, 2, 249-290. https://doi.org/10.1201/9780203713297

Rolland, L. M., P. Lognonné, & H. Munekane (2011). Detection and modeling of Rayleigh wave induced patterns in the ionosphere, Journal of Geophysical Research, 116, A05320. https://doi.org/10.1029/2010JA016060

Schnepf, N. R., Manoj C., An, C., Sugioka, H. & Toh, H. (2016). Time-frequency characteristics of tsunami magnetic signals from four Pacific Ocean events. Pure and Applied Geophysics, 173:3935–3953. https://doi.org/10.1007/s00024-016-1345-5

Zettergren, M. D., & Snively, J. B. (2013). Ionospheric signatures of acoustic waves generated by transient tropospheric forcing. Geophysical Research Letters, 40(20), 5345-5349. https://doi.org/10.1002/2013GL058018

Zettergren, M. D., & Snively, J. B. (2015). Ionospheric response to infrasonic-acoustic waves generated by natural hazard events. Journal of Geophysical Research: Space Physics, 120(9), 8002-8024. https://doi.org/10.1002/2015JA021116